Foaming parameter identification of polyurethane using FOAMAT ® device

Clément Raimbault, Patrice Laure, Guillaume François, Séverine Boyer, Michel Vincent, François Choquart, Jean-François Agassant

Foaming parameter identification of polyurethane using FOAMAT® device

C. Raimbault[1,3], P. Laure[1,4], G. François[2], S.A.E. Boyer[1], M. Vincent[1], F. Choquart[3], J.F. Agassant[1]

(1) MINES Paristech, PSL Research University, CEMEF, UMR CNRS 7635, Sophia-Antipolis, 06560 Valbonne, France

(2) Transvalor, Sophia-Antipolis, 06410 Biot, France

(3) Trèves PSI, 51686 Reims, France

(4) Univ. Côte d'Azur, CNRS, Lab. J.A. Dieudonné, UMR CNRS7351, Parc Valrose F-06000 Nice, France

Highlights:

- New modeling equations for polyurethane foaming which can be fully identified with FOAMAT® device.
- New analytical solution describing flow motion inside FOAMAT® device.
- Analysis of the influence of viscosity modeling on foaming simulation.

Abstract: A key problem in the modeling of polyurethane foaming is the determination of relevant physical parameters for the viscosity, the gas expansion and the curing rate. Indeed, it is difficult to measure the chemical kinetics parameters as well as the viscosity of industrial polyurethane formulations (polyol-isocyanate-water mixture) because the time scales of gas production and polyurethane crosslinking are very short and hardly compatible with the installation of the sample in characterization devices such as DSC and parallel plates rheometer. A FOAMAT® system has been developed to get these experimental data but the relationship between measurements and rheo-chemical parameters has not been clearly established. In this paper an analytical model of the foaming process is developed in the cylindrical FOAMAT® geometry which allows identifying the parameters of the curing and gas production kinetics equations, as well as the viscosity. This analytical model is based on a set of simplifying hypotheses which validity is checked using the finite element computation software REM3D® dedicated to foaming modelling and applicable for injection-molding processing.

Keywords: Polyurethane, Foam, FOAMAT® experiments, Foaming and Curing Kinetics, Rheology, Modelling

1. Introduction

Polyurethane (PU) foams are produced by mixing polyol, isocyanate and a blowing agent such as water. Two main chemical reactions are in competition: isocyanate and water produce carbon dioxide (CO_2) that governs the development of bubbles. The crosslinking reaction between isocyanate and polyol produces the solidification of the polyurethane skeleton. The quality of the foam (bubble size and density) depends on the coupling between these two reactions. If the crosslinking reaction starts too early, the viscosity of the skeleton increases and blocks the foam expansion. On the other hand, if the crosslinking reaction starts too late, the foam collapses because the structure of the skeleton is not strong enough.

Injection molding of polyurethane foam is a complex process. A certain quantity of a Polyol-Isocyanate-Water mixture (PIW) is injected in the mold cavity that is of course only partially filled. The blowing reaction leads to a volume increase and complete cavity filling. The process is unsteady and non-isothermal. It involves flow, heat transfer and chemical reactions. Gravity needs to be accounted for. The challenge is to predict the ability of the foam to fill all the regions of the cavity and the final density and microstructure (bubbles shape and size distributions) on which properties such as acoustic, thermal insulation will depend. Several commercial softwares help designing molds and selecting processing parameters. They are based on physical models for the foam rheology, the foaming and curing reactions, and the heat transfer. All these models require identification of numerous parameters.

Several kinetics models [1] [2] account directly for chemical reactions between isocyanate and polyol on one side and isocyanate and water on the other side. Additional chemical reactions with surfactants and other additives can also be considered. The evolution of density is expressed as a function of the different species [3,4]. Various phenomenological kinetics equations have been proposed for the foaming and curing reactions in [5-7] [8, 9].

The conversion rate of the curing reaction β has been obtained by [10] with Differential Scanning Calorimetry (DSC) analysis in isothermal and non-isothermal modes for non-foamed PU formulations. Bouayad *et al.* [11] used DSC analysis in isothermal mode for PU foams to identify both foaming and curing reactions with a specific formulation where these reactions are not superimposed. In most industrial formulations, the measurement of the conversion rate of the blowing reaction α is more difficult and several foam expansion models approximate the volume variation $V(t)$ by a formula fitted from experimental data obtained for self-expanding foam in a cylindrical set-up [12]. In the same way, other authors [13,14] suggested an empirical formula fitted from experimental data which expressed the evolution of the density of foam mixture. The issue is to apply this empirical formula for any mold and any processing conditions.

A key parameter is the rheology of PU formulations during curing and foaming. The studies on bubble growth surrounded by a reacting fluid [15] [16] pointed out the importance of the viscosity on the final porosity of a solid foam. Additional studies [17] [18] have shown that viscosity has an influence only at the early stage of bubble growth but then, as soon as the viscosity is important, it is controlled by gas diffusion from the liquid to the bubble and is driven by diffusivity and Henry's law parameters. When considering a population of bubbles, Ferkl *et al.* [16] have shown that the viscosity has an influence on the wall thickness between bubbles before coalescence and especially to the transition from closed bubbles to open bubbles.

The first rheology equations for thermoset polymers have been proposed in [9, 19, 20] and applied to epoxy resins. Other constitutive equations have been proposed in refs. [7] and [21] for PU formulations. They have been extended by Bikard et al. [22] to foamed PU formulations.

Rheology measurements of non-foamed PU during curing have been performed [10] with a parallel-plate rheometer. Measuring the rheology of PU formulations during foaming in this type of rheometer is a challenge for two reasons. First, the velocity field is two-dimensional [11, 23, 24]. In [11] a specific analysis of the compressible flow of the foam in a parallel plate

rheometer is developed which defines specific dynamic conditions to obtain a dominant orthoradial shearing flow. The second difficulty for the rheology measurement is related to short reaction time of industrial formulations compared to sample placement in the rheometer. Therefore, other techniques have been used. Tuarez *et al.* [25] measured the viscosity of an isocyanate/polyol mixture during the polymerization of a urethane pre-polymer using a rheo-reactor constituted of a cylindrical vessel with a helical ribbon impeller. Isocyanate and polyol are poured in the vessel and mixed by the ribbon impeller rotating at a prescribed velocity. A mean shear rate in the vessel is calculated and the viscosity as a function of time deduced from the torque measurement on the vessel as explained in [26]. This rheo-reactor cannot be applied to the huge viscosity increase encountered during the polymerization kinetics of polyurethane or polyurethane foam.

In order to overcome these limitations, we have used a FOAMAT® system (Format Messtechnik GmbH) to get experimental data [27]. It consists in a cylindrical reservoir equipped with a thermocouple and a pressure transducer. The mixture is introduced in the reservoir. The foaming dynamics (the height of the sample as a function of time) and the temperature and pressure evolutions are simultaneously measured. The issue is to derive relevant chemical kinetics and rheology parameters from these FOAMAT® measurements.

Several numerical models have been developed to predict PU foam expansion in industrial mold geometries using both macroscale modeling [22][28-30] and microscale modeling [15, 31, 32] [33-35]. In [22] a macroscale numerical simulation of foam expansion using REM3D® is applied to the cylindrical geometry of the specially developed RHEOFOAM system which is very similar to the FOAMAT®.

In this paper, the FOAMAT® experiments are described and discussed in Section 2. Foaming and curing equations are presented in Section 3. An analytical resolution of the set of equations in the FOAMAT® set-up is presented in Section 4 as well as an identification methodology of the kinetics and rheology parameters. The foaming model that we develop is based on several hypotheses that are discussed and justified by comparing its results with numerical computations using REM3D® foaming software in Section 5.

2. FOAMAT® measurements

The FOAMAT® system (Fig. 1) consists of a cardboard container (radius $R = 0.075\,m$, height $0.18\,m$, wall thickness $3\,mm$). Polyol, isocyanate and water are first mixed in a separate container and then the mixture is poured in the bottom of the container. The mass of the poured mixture varies between 0.110 and $0.115\,kg$ corresponding to an initial height in the cardboard container in the range of 5.75 and $6.01\,mm$ (the initial density of the mixture is $\rho_0 = 1082\,kg/m^3$). Three measurements are carried out:

- An ultrasonic sensor (LR 2-40 PFT, $0.1\,mm$ resolution) allows measuring the evolution of the height H of the free surface on the axis of symmetry as a function of time ($H(t) = h(0,t)$). The height is lower elsewhere as the free surface is not flat. An air jet is applied to the upstream surface of the foam during the whole experiment in order to homogenize the air volume between the sensor and the PU free surface for reliable sound propagation conditions.

- The PU temperature T_{TC} is measured with a type K thermocouple introduced in the container at the end of foam rising at a height of $0.05\ m$. The time of introduction is chosen not to interfere with the foam upper surface motion. The drawback is that there is no temperature data during most of expansion time.

- The force on the whole bottom of the container is measured with a $500\ N$ force gauge and gives an average stress $\bar{\sigma}_{zz}$.

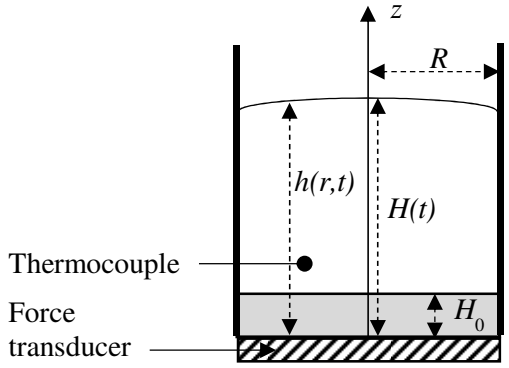

FIGURE 1: Scheme of the FOAMAT® system

Figures 2 show typical measurements for a PIW mixture at three different initial temperatures (23, 28 and $34\ °C$). The measurements are made on an industrial formulation as the scope is to propose a methodology for a real product. Two experiments have been performed at each temperature. The reproducibility is good for the foam height (Fig. 2a), foam rise velocity dH/dt (that is deduced from height measurements) (Fig. 2c) and temperature (Fig. 2b). The stress (Fig. 2d) is less reproducible and its order of magnitude is very low (several hundred Pascal).

Three time-scales can be identified:

- A time scale $[10 - 60\ s]$ for the height evolution (Fig. 2a). The foam height increases between $10\ s$ and $35 - 55\ s$ depending on the temperature of work. A small decrease of the height can be observed before stabilization at around $60\ s$.
- A time scale $[10 - 140\ s]$ for the stress measurement (Fig. 2d). At the beginning the stress is related to the weight of the PIW mixture, it increases and reaches a maximum and then it decreases progressively towards 0, meaning that the weight of the foam is no more measured by the transducer.
- A time scale for the temperature measurement $[30 - 600\ s]$ (Fig. 2b). The temperature increases suddenly at the introduction time of the thermocouple (which is obviously not reproducible but corresponds more or less to the final foam rising time) and then continues to increase sharply till 100 s, more smoothly till around 300 s and then decreases till demolding time ($600\ s$).

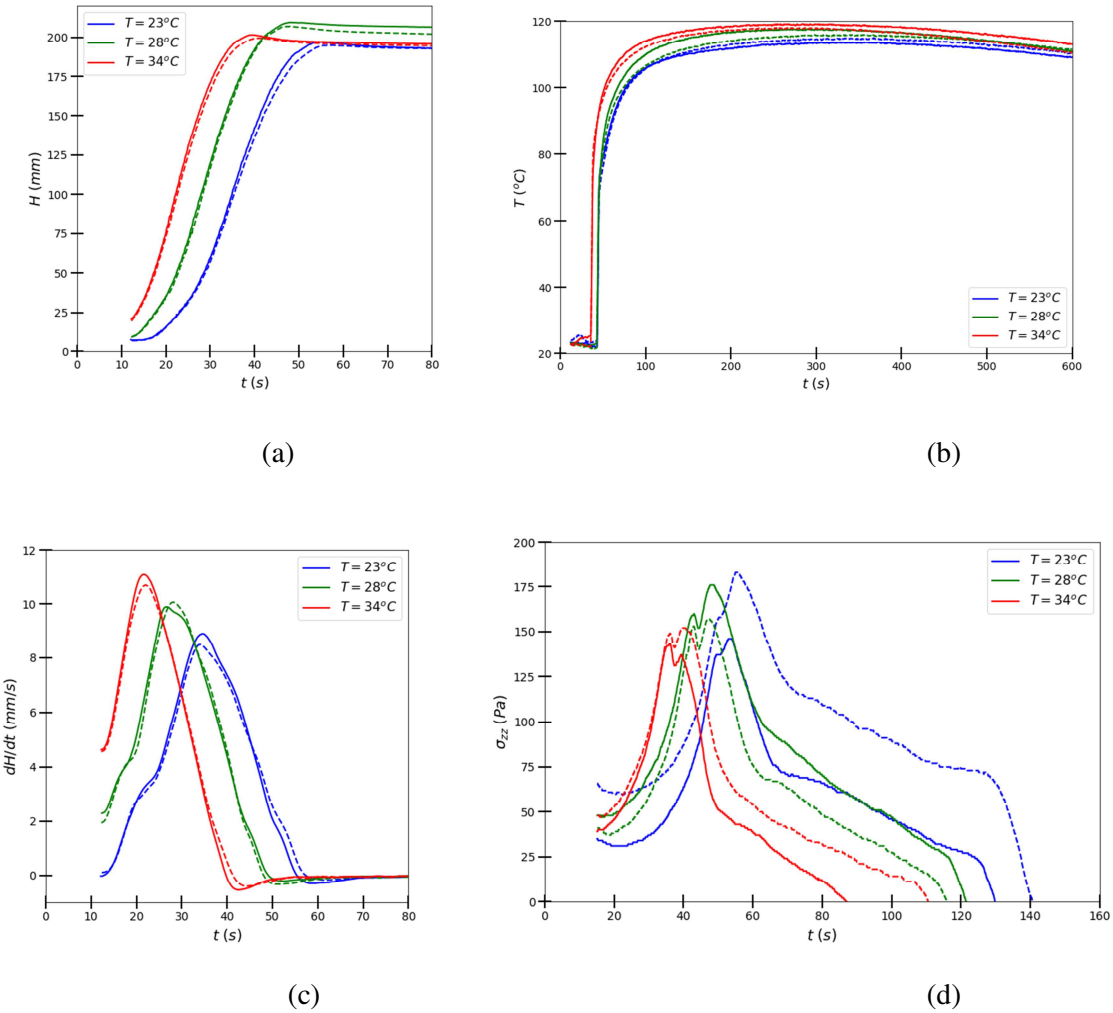

FIGURE 2: Typical measurements made with the FOAMAT®: (a) height H; (b) temperature T; (c) vertical velocity dH/dt of the foam/air interface measured on the axis of symmetry of the container; (d) vertical average stress normal to the bottom. In the sequel, only the solid lines are plotted in Figures explaining the parameter identifications.

The time at which the stress is maximum corresponds exactly to the time when the height reaches a maximum. For initial PIW temperatures of 34 °C and 28 °C , the thermocouple temperature starts to increase at the maximum height time, respectively 36 s and 43 s, which points out that the thermocouple is introduced when foam rising is completed. For an initial PIW temperature of 23 °C, the thermocouple has been introduced before foam rising completion (43 s instead of 53 s). The conclusion is that the temperature evolution cannot be used directly to determine the heat generated by the foaming reaction. In figure SM1 of supplementary material the stress and temperature measurements are plotted on the time scale [0-80s] in which the foaming is done.

3. Foaming equations

The most suitable approach to model foaming seems to be a diphasic one [32]. The evolution of each component (polymer and immiscible bubble) is governed by specific equations (namely the Stokes equation for polymer and ideal gas for bubbles). The number of moles in each bubble is linked to the conversion rate. The polymer viscosity depends on the curing reaction according to a Piloyan law [5] and follows the model developed by Castro *et al.* [7].

This diphasic approach can be used to build a macroscopic model for foam mixture presented hereafter and usually used in direct numerical simulation. The following equations for the conservation of mass, momentum and energy are usually used [2, 12] [22, 23, 30, 36].

The mass balance can be expressed in term of foam volume variation $V(t)$ [12] or gas content ϕ [22] and writes:

$$\nabla . \boldsymbol{u} = -\frac{1}{\rho}\frac{d\rho}{dt} = \frac{1}{V(t)}\frac{dV(t)}{dt} = \frac{1}{1-\phi}\frac{d\phi}{dt} \tag{1}$$

where ρ is the density, $\boldsymbol{u}$ is the velocity and assuming that $\rho = \phi\rho_{co_2} + (1-\phi)\rho_{pu} \sim (1-\phi)\rho_{pu}$ (as the density of CO_2 is one hundred time smaller than that of polyurethane).

The momentum balance is given by:

$$\frac{\partial}{\partial t}(\rho\,\boldsymbol{u}) + \nabla.(\rho\,\boldsymbol{u}) = \nabla.\boldsymbol{\sigma} + \rho\,\boldsymbol{g} \tag{2}$$

where $\boldsymbol{\sigma}$ is the stress tensor, $\boldsymbol{g}$ is the acceleration due to gravity. For a slightly compressible material the bulk viscosity may be neglected and $\boldsymbol{\sigma}$ writes:

$$\boldsymbol{\sigma} = -p\,\mathbf{I} + 2\eta\left(\dot{\boldsymbol{\varepsilon}} - \frac{1}{3}\mathrm{tr}\dot{\boldsymbol{\varepsilon}}\,\mathbf{I}\right) \tag{3}$$

$\dot{\boldsymbol{\varepsilon}}$ is the rate of strain tensor, $\mathbf{I}$ is the identity tensor, p is the pressure and η the viscosity which is a complex function of temperature, curing kinetics and gas creation kinetics as depicted in Equation (9). It is classical formulation for compressible fluid assuming that the viscosity follows a compressible Newtonian behavior [37].

The temperature evolution is given by the energy balance equation:

$$\rho\,C_p\left(\frac{\partial T}{\partial t} + \boldsymbol{u}\,.(\nabla T)\right) = \nabla\cdot(\kappa\nabla T) + p\nabla\cdot\boldsymbol{u} + \eta\,\dot{\bar{\varepsilon}}^2 + \chi\,\frac{dp}{dt} + \Delta H_{\mathrm{PU}} + \Delta H_{\mathrm{foam}} \tag{4}$$

where C_p is the specific heat, κ the thermal conductivity, χ is the foam compressibility coefficient, ΔH_{PU} is the heat generated during the polymerization reaction and ΔH_{foam} the heat generated during the foam formation. C_p and κ are functions of the gas content using a linear mixing rule.

The coupling with chemical reactions (CO_2-bubbles expansion and polymerization) is modeled in different ways according to authors. A well-accepted approach assumes that both reactions are governed by chemical kinetics and follow Piloyan laws [5] [23, 38].

The usual curing kinetics equation [22, 23] writes:

$$\frac{d\beta}{dt} = K_\beta \exp\left(\frac{E_\beta}{R_g}\left[\frac{1}{T_{ref}} - \frac{1}{T}\right]\right) \beta^{m_\beta} (1 - \beta)^{n_\beta} \tag{5}$$

where β is the conversion rate, E_β is the activation energy, T_{ref} is a reference temperature, K_β, m_β and n_β are material parameters. Note that other equations are proposed in the literature as first order kinetics [39][40], second order kinetics [3] [4] [8] or Kamal cure model [6] [12]. The equation in ref. [8] is a special case of Equation (5) with $m_\beta = 0$ and $n_\beta = 2$.

The heat generation due to curing reaction is then written as follow:

$$\Delta H_{\mathrm{PU}} = \delta H_\beta \frac{d\beta}{dt} \tag{6}$$

where δH_β is the enthalpy of the curing reaction.

In the same way, the Piloyan law for the gas conversion rate α is:

$$\frac{d\alpha}{dt} = K_\alpha \exp\left(\frac{E_\alpha}{R_g}\left[\frac{1}{T_{ref}} - \frac{1}{T}\right]\right) \alpha^{m_\alpha} (1 - \alpha)^{n_\alpha} \tag{7}$$

Abdessalam *et al.* [38] assumed that $m_\alpha + n_\alpha = 2$.

The gas is assumed to follow the ideal gas law. Therefore, the evolution of the gas fraction ϕ can be expressed as [22]:

$$\frac{1}{\phi(1-\phi)} \frac{d\phi}{dt} = \frac{1}{\alpha}\frac{d\alpha}{dt} + \frac{1}{T}\frac{dT}{dt} - \frac{1}{p}\frac{dp}{dt} \tag{8}$$

A viscosity model has been proposed in refs [7] and [21] for PU formulations and extended to PU foaming formulations [22]. It is assumed that the viscosity is split in three parts: the Arrhenius law describes the dependence with temperature; the function F_g gives the influence of gas content on viscosity; the function F_p describes the increase of viscosity with the curing reaction:

$$\eta = \eta_0 \exp\left(\frac{E_\eta}{R_g}\left[\frac{1}{T_{ref}} - \frac{1}{T}\right]\right) F_g(\phi)\ F_p(\beta) \tag{9}$$

where E_η is the activation energy for the viscosity, R_g is the ideal gas constant, η_0 is the viscosity of the PIW mixture at the reference temperature T_{ref} before curing.

The function F_g associated to gas production is usually written as follows:

$$F_g(\phi) = a_0 + a_1\phi + a_2\,\phi^2 \tag{10}$$

as it derives from the generalized Einstein equation [41] initially established for spherical solid particles in a Newtonian fluid. The coefficient a_1 which is positive for solid particles is negative for foam because of the fluidizing effect of gas bubbles. Equation (10) can also be considered as a simplification of the theoretical model proposed in [42] for foams. A set of values proposed in ref. [22] ($a_1 = -1.2$ and $a_2 = 0.5$) is used for numerical simulations in ref. [12]. Others authors [42][43] proposed alternative approaches based on the physics of emulsions [31] [37].

Two main approaches are proposed in the literature to determine the function F_p giving the influence of the curing kinetic on viscosity without a detailed knowledge of the material chemistry.

The first approach is an extension of the percolation model for the gelation of thermosetting resins [44]. It writes:

$$F_p(\beta) = \left(\frac{\beta_c}{\beta_c - \beta}\right)^{\gamma(\beta)} \quad ; \quad \gamma(\beta) = b_0 + b_1\beta \tag{11}$$

where β_c is a critical curing rate and γ a power factor which depends on the curing rate. Estimations of critical curing rate β_c as well as fitted values of b_0 and b_1 can be found in refs [10, 12, 45-49].

The second approach, initiated by Roller [19] for epoxy resin, proposes a simple form of the percolation model, namely $F_p = 1/(1-\beta)$. Thus, the evolution of viscosity as a function of both time and temperature is expressed as follows if F_g is not considered:

$$\ln \eta(t,T) = \ln \eta_0 + \frac{E_\eta}{R_g}\left[\frac{1}{T_{ref}} - \frac{1}{T}\right] + K_0 \int_0^t \exp\left(\frac{E_K}{R_g}\left[\frac{1}{T_{ref}} - \frac{1}{T}\right]\right) dt \tag{12}$$

for a first order curing reaction and

$$\ln \eta(t,T) = \ln \eta_0 + \frac{E_\eta}{R_g}\left[\frac{1}{T_{ref}} - \frac{1}{T}\right] + \ln\left[1 + K_0 \int_0^t \exp\left(\frac{E_K}{R_g}\left[\frac{1}{T_{ref}} - \frac{1}{T}\right]\right) dt\right] \tag{13}$$

for a second order curing reaction [22]. In Equations (12-13) the second term corresponds to the Arrhenius law already present in Equation (9). The third term, also defined by an Arrhenius law with parameters (K_0, E_K), is an "apparent kinetic" factor [20] of the percolation model. Measurements made on epoxy resin [9, 19] showed that the fitting values for (K_0, E_K) are larger than kinetic constants determined via DSC. This approach will be used in this paper.

This set of equations (1-7) and (12) will be modified in the next section to adapt the modelling to the experimental limitations imposed by the FOAMAT® device.

4. Identification of the parameters with FOAMAT® setup

4.1 Identification of curing kinetics parameters

In the energy balance equation (Equation (4)), the dissipation due to compressibility (second and fourth terms of the right-hand side) and the viscous dissipation (third term) are neglected due to the low pressure (Figure 2d) and the low foam rising velocity (Figure 2c). As a consequence, Equation (4) becomes:

$$\rho\, C_p \frac{dT}{dt} = \nabla.(\kappa\, \nabla T) + \Delta H_{\mathrm{PU}} + \Delta H_{\mathrm{foam}} \tag{14}$$

Figure 2b shows that the FOAMAT® is not adiabatic as the temperature decreases for a large time. Equation (14) can be re-written with average values ($\bar{T}$ and $\Delta\bar{H}_{\mathrm{PU}}$) on the foamed volume:

$$\rho\, C_p \frac{d\bar{T}}{dt} \pi\, R^2 H(t) = \; h_T\, (T_{amb} - \bar{T})\, \pi\, R^2 + \Delta\bar{H}_{\mathrm{PU}}\; \pi\, R^2 H(t) \tag{15}$$

The variable $H(t)$ is the average height of the foam in the FOAMAT® at time *t* which can be chosen as the height measured on the FOAMAT® symmetry axis. This means that the curvature of the free surface is neglected. The term h_T is the heat transfer coefficient by convection through the free surface. The heat transferred by conduction through the bottom plaque and the cardboard wall is neglected in front of the heat transfer due to forced convection applied by the air jet at the foam surface. T_{amb} is the temperature of the air jet. $\Delta\bar{H}_{\mathrm{PU}}$ is the average energy created by the curing reaction per unit volume at a given time t. The heat generated by the foaming reaction ΔH_{foam} is not considered because it cannot be measured in the FOAMAT® device (see Section 2). Equation (15) can thus be rewritten as:

$$\frac{d\bar{T}}{dt} = \frac{h_T}{\rho\, C_p H(t)} (T_{\mathrm{amb}} - \bar{T}) \; + \frac{\Delta\bar{H}_{\mathrm{PU}}}{\rho\, C_p} = \; c_f\, (T_{amb} - \bar{T}) + \frac{dT_{\mathrm{ad}}}{dt} \tag{16}$$

where the transfer coefficient $c_f = h_T/(\rho\, C_p H(t))$ varies as a function of time during foam rising, that is, according to Figure 2a, until around $50\ s$. Then H and $\rho\, C_p$ remain constant in the range $[50 - 600\ s]$ and therefore c_f. This last value will be chosen in the following discussion. The term T_{ad} is the foam temperature that would be in the system if the conditions were adiabatic ($c_f = 0$). The curing rate β can be linked to T_{ad} by Equation (17):

$$\beta = \frac{T_{\mathrm{ad}} - T_0}{T_{\mathrm{ad}}^m - T_0} \tag{17}$$

where T_{ad}^m is the maximum temperature reached for an initial temperature T_0. The curing rate is assumed to follow a second order law:

$$\frac{d\beta}{dt} = \; K_\beta \exp\left(\frac{E_\beta}{R_g}\left[\; \frac{1}{T_{\mathrm{ref}}} - \frac{1}{T}\right]\right)(1 - \; \beta)^2 \tag{18}$$

And therefore Equations (17) and (18) lead to:

$$\frac{dT_{\mathrm{ad}}}{dt} = \; K_{\mathrm{ad}} \left(\frac{T_m - T_{\mathrm{ad}} + \; T_0 - \; T_{\mathrm{ref}}}{T_m - T_{\mathrm{ref}}}\right)^2 \exp\left(\frac{E_{\mathrm{ad}}}{R_g}\left(\frac{1}{T_{\mathrm{ref}}} - \frac{1}{T}\right)\right) \tag{19}$$

where $K_{\mathrm{ad}} = K_\beta\, (T_{\mathrm{ad}}^m - \; T_0)$ and $E_{\mathrm{ad}} = E_\beta$. The parameter $T_m = T_{\mathrm{ref}} + T_{\mathrm{ad}}^m - \; T_0$ replaces T_{ad}^m. In this way, this new parameter depends only on a reference temperature T_{ref}.

We assume that the temperature is nearly homogenous in the volume, $\bar{T} = \; T(r, z)$, even during the cooling step so that the average temperature is equal to the temperature at the thermocouple position: $\bar{T} = \; T(r = 0, z = 50\ \mathrm{mm}) = T_{\mathrm{TC}}$. This will be checked in section 5 by means of direct numerical computations. Finally, Equation (16) becomes:

$$\frac{dT_{\mathrm{TC}}}{dt} = \; \frac{dT_{\mathrm{ad}}}{dt} + (T_{\mathrm{amb}} - T_{\mathrm{TC}})\, c_f \tag{20}$$

The experiments are made at ambient temperature $T_{\mathrm{amb}} = 20$ °C and $T_{\mathrm{ref}} = 21$ °C is chosen. A fitting procedure applied to the experimental temperature traces of Fig. 2b at the three initial temperatures ($T_0 =$ 23, 28 and 34 °C) leads to values reported in Table 1. From the identified kinetics coefficients $(K_{\mathrm{ad}}, E_{\mathrm{ad}}/R_g)$ one derives $(K_\beta, E_\beta/R_g)$ values of the same order of magnitude as those identified in [11] ($K_\beta = 10^{-2}$ s^{-1}; $E_\beta/R_g = 1000$ K).

Figure 3 compares the evolution of the adiabatic temperature T_{ad} and the global temperature, calculated with these identified values, to the experimental one. As noted before, the experimental measurements are not available at the early stage of the process because the temperature starts to be measured only around the maximum foam rising time. During this early stage the model shows a sharp increase. Then the adiabatic temperature continues to increase till the end of the process whereas the measured temperature decreases during the foam consolidation. This is accounted for when introducing the heat transfer coefficient c_f and the agreement between the computed and the measured temperatures is nice. Note that the first part of the curve ($0 < t < 50\ s$) where the temperature measurement is not available will be used in section 4.2 for the foaming rate identification.

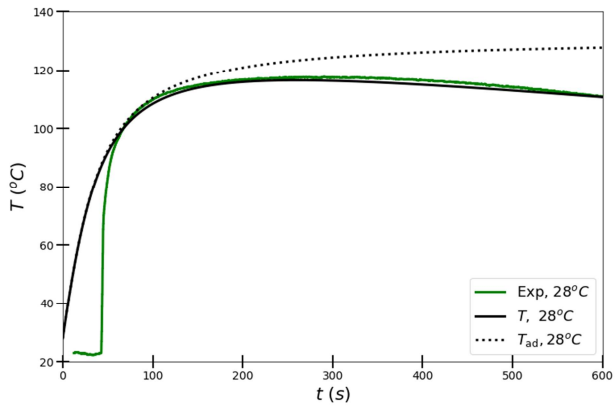

FIGURE 3: Experimental data and fitting curves for initial temperatures $T_0 = 28$ °C

4.2 Identification of gas expansion kinetics.

4.2.1 Definition of the gas content ϕ_{free} at ambient pressure

The gas content ϕ at time t is a function of the pressure and the temperature at time t, and the number of moles of gas created between 0 and t, denoted respectively $p(t), T(t), n(t)$. It is supposed to be homogeneous at each time step in the foamed volume, which means that the density $\rho(t)$ is homogeneous too at each time step. This assumption is consistent with the assumption of homogeneous temperature in the volume. Moreover, this implies that the porosities that develop during foaming remain closed or (and) that there is no gas diffusion through the outer surface of the foamed part. The number of moles $n(t)$ depends on the temperature history $T(\tau)$ for $0 < \tau < t$. The gas content ϕ is defined in general pressure and temperature conditions by:

$$\phi\big(p(t), T(t), n(t)\big) = \frac{V_g\big(p(t), T(t), n(t)\big)}{V_{\mathrm{foam}}} \tag{21}$$

where V_g is the volume of gas contained in the volume of foam V_{foam}. During a FOAMAT® experiment, the pressure increase remains limited (see Fig. 2d) and therefore p is assumed to be constant and equal to the atmospheric pressure p_a. The temperature increases, however it remains homogeneous at each time step if the heat exchange with the surrounding is neglected, so that a gas fraction ϕ_{free} at ambient pressure is defined:

$$\phi_{\text{free}}(t) = \phi\big(p_a, T(t), n(t)\big) \tag{22}$$

In a FOAMAT® experiment, $\phi_{\text{free}}(t)$ is directly related to the foam volume which is known thanks to the foam height transducer and to the polyurethane volume which is assumed to be constant and equal to the initial volume of the PIW mixture.

4.2.2 Identification of gas expansion at ambient pressure in the FOAMAT®

Assuming that the free surface remains flat during foam rising, $(h(r,t) = h(0,t) = H(t))$, the relation between the gas content ϕ_{free} and the foam height H at any time is:

$$\phi_{\text{free}}(t) = 1 - \frac{H_0}{H(t)} \tag{23}$$

with H_0 the initial height of the PIW mixture before expansion. There is an initial gas content in this mixture which corresponds to the air entrapped after the thorough mixing of polyol, isocyanate and water. However, we assume in the following that this initial gas content is negligible.

We assume a kinetics law for the gas content evolution of the same type as the gas conversion rate Equation (7):

$$\frac{d\phi_{free}}{dt} = f\left(\phi_{free}, T\right) = K_\phi \exp\left(\frac{E_\phi}{R_g}\left(\frac{1}{T_{ref}} - \frac{1}{T}\right)\right) \phi_{\text{free}}^{m_\phi} \left(\phi_{\max} - \phi_{\text{free}}\right)^{n_\phi} \tag{24}$$

$\phi_{\max}$ is the maximum gas content which does not depend on the initial temperature, but only on the initial composition of the PIW mixture. It corresponds to the final value reached in the foam when bubble opening occurs. After this transition, the gas captured inside the bubbles is partially evacuated and the bubbles stop growing. The experimental foam rising dynamics (Fig. 2a) and the computed temperature development (Fig. 3) allow identifying the values of ($\phi_{\max}$, K_ϕ, E_ϕ/R_g, n_ϕ, m_ϕ) by the fitting procedure already used in section 4.1. Figure 4 shows that the model predicts quite accurately the measured height. The gas fraction as a function of time is presented in Figure SM 2a of supplementary material. The values of the parameters are reported on Table 1

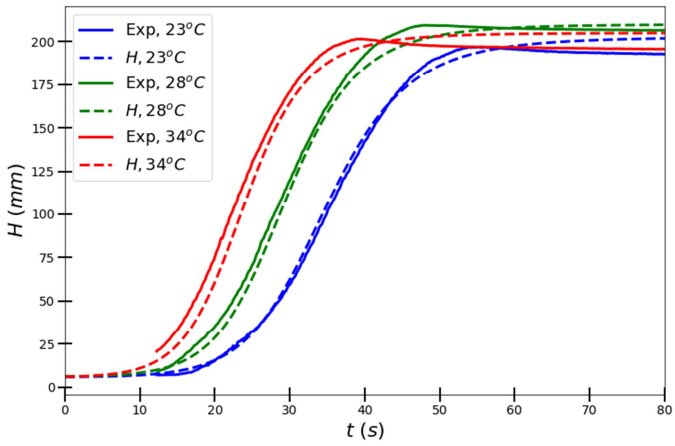

FIGURE 4: Experimental data and fitting curves of the height evolution for the three initial tested temperatures

4.2.3 Relation between the conversion rate α and the gas content ϕ_{free}

Using the ideal gas law for CO_2, the number n of gas mole created at constant atmospheric pressure is:

$$n(t) = \frac{p_a V_g}{R_g T} = \frac{V_{PU}}{R_g} \frac{\phi_{\text{free}}}{1-\phi_{\text{free}}} \frac{p_a}{T} \tag{25}$$

One can define the conversion rate of gas reaction α, as follows:

$$\alpha = \frac{n}{n_{\max}} = \left(\frac{\phi_{\text{free}}}{\phi_{\max}}\right)\left(\frac{1-\phi_{\max}}{1-\phi_{\text{free}}}\right) \frac{T(H_{\max})}{T} \tag{24}$$

where n and $n_{\max}$ are respectively the number of moles of gas at time t and at the end of the reaction. $T(H_{max})$ is the temperature of the foam when foam rising is completed. The maximum gas content $\phi_{\max}$ has been determined previously.

From the values of ϕ_{free} (Fig SM2a of the supplementary material) and T (Fig. 3) as a function of time and the experimental value of $T(H_{\max})$, one can deduce $\alpha(t)$ for the three different temperatures.

The curves of Figure SM2b of supplementary material can be fitted by Equation (7) and keeping $m_\alpha = m_\phi$ (0.094) and $n_\alpha = n_\phi$ (1.535), one gets $K_\alpha = 0.05\ s^{-1}$ and $E_\alpha/R = = 5373$ K. These values are of the same order of magnitude as the kinetics parameters identified by [31][38], namely, $m_\alpha = m_\phi = 0.088$, $n_\alpha = 1.3$ and $K_\alpha = 0.04\ s^{-1}$.

Therefore, from FOAMAT® measurements, it is possible to compute parameters of Equation (7) describing the evolution of gas conversion rate.

4.3 Viscosity Identification

The proposed analytical model is based on a set of hypotheses some of which have been introduced in sections 4.1 and 4.2: both temperature and foam density are homogeneous in the

whole volume at each time step; the free surface of the foam is flat; the velocity field is axisymmetric; the vertical velocity component varies linearly with the vertical coordinate z, the foam sticks to the cylinder wall.

The compressible Stokes equations (Equations (1-3)) are analytically solved to obtain the pressure and the velocity and stress components. The calculations are developed in Section 3 of supplementary material. Equation (27) (A-21 in SM3) gives the evolution of the viscosity at each time during foam rising as a function of the average stress $\bar{\sigma}_{zz}$ measured on the bottom of the FOAMAT®, of the foam height $H(t)$, of the foam rising velocity $dH(t)/dt$ and of the mass m of the PIW mixture.

$$\eta(t) = \frac{\bar{\sigma}_{zz}(0,t) - \frac{m\,g}{\pi\,R^2}}{\frac{1}{H(t)}\,\frac{dH(t)}{dt}\left[2\,\frac{H^2(t)}{R^2} + \frac{3}{2}\right]} \tag{25}$$

All those data are experimentally measured (Fig 2). Figure 5 shows the viscosity evolution deduced from Equation (27). The curves start when the measured stress overcomes the stress associated to the weight of the PIW mixture. There is a sharp initial increase, then a linear increase in a logarithmic scale and finally the viscosity grows towards infinity when the foam rise stops i.e. dH/dt=0 (see Fig. 2a). At that time the stress sensor should measure the PU weight so that the numerator should also be zero and therefore the viscosity should be finite. Fig. 2d shows that it is not the case. Other phenomena should take place: viscoelastic relaxation of the polyurethane, sticking contact along the cardboard wall of the FOAMAT® during the foam retraction (see Fig. 2a), and gas escape when the cells get connected [24]. Consequently, the viscosity measurement is only possible with the FOAMAT® on a restricted time scale. When the foam rise is achieved, the temperature continues to increase which points out that the curing reaction is not completed. That means that the viscosity, even very high, remains limited. As a conclusion, Equation (27) is valid only when the foam flows *i.e.* when $\bar{\sigma}_{zz} > mg/\pi R^2$ and $dH/dt > 0$. It cannot be used to determine the viscosity evolution during the last part of curing.

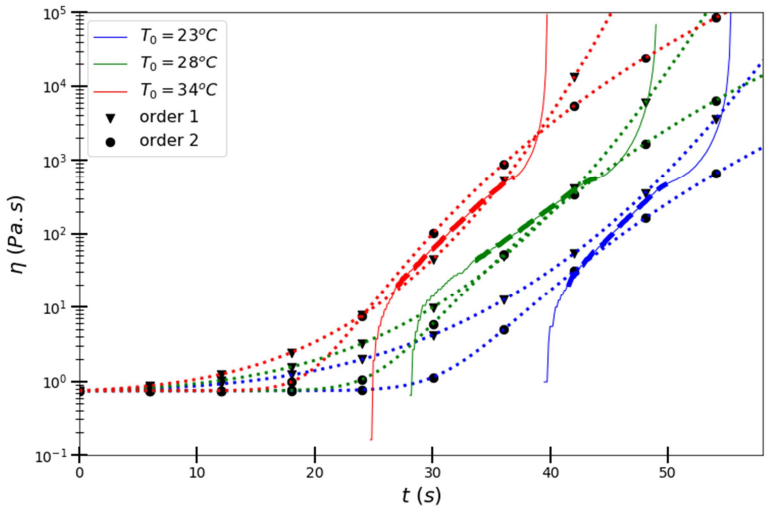

Figure 5: Viscosity as a function of time for three initial PIW temperatures: solid lines correspond to experimental data deduced from Equation (27); dashed lines corresponds to the restricted data domain used to identify the viscosity behavior, either with Equation (28) (triangle) or Equation (29) (dot)

At each time step of Figure 4 we define from Equation (18) the curing kinetics parameter β and from Equation (24) the gas content ϕ . Fig. 6 shows that the time interval corresponds to a limited range of curing kinetics ($0.4 \leq \beta \leq 0.6$) and of foaming kinetics ($\phi \sim 0.96$) very near the maximal gas content $\phi_{\max}$ (0.971). Therefore, these available data do not allow an accurate fitting of all coefficients used in Equations (9-12) and (13).

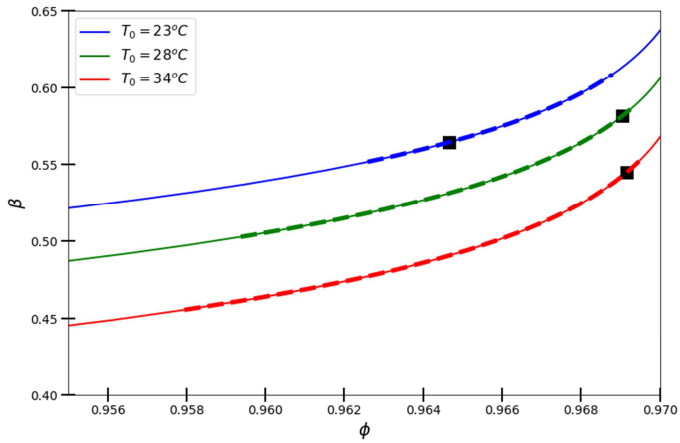

FIGURE 6: Parameter ranges in which the viscosity is experimentally measured: solid lines correspond to fitted curves obtained in previous sections; the squares indicate the smallest values from which the temperature and therefore β are experimentally known; dashed lines correspond to values reached during viscosity measurements: $\phi \sim 0.96$ *and* $0.4 \leq \beta \leq 0.6$ or $75\ °C \leq T \leq 87.5\ °C$.

However, it is important to notice that, if the viscosity and the gas content are only measured during the foam rising time when there is a flow motion, the temperature is measured on a wider time scale which allows identifying curing kinetics parameters till the end of the curing process. As the logarithm of the measured viscosities (dashed lines in Fig. 5) increases linearly with time we have used the methodology already proposed for epoxy resins [9, 19, 50, 55].

The viscosity can be approximated by a simplified form of Equation (12):

$$\ln \eta = \ln \eta_0 + K(T_{ad})\, t \tag{26}$$

or Equation (13):

$$\ln \eta(t,T) = \ln \eta_0 + \ln[1 + K(T_{ad})\, t] \tag{29}$$

for curing kinetics reactions of order 1 or 2 respectively.

The adiabatic temperature T_{ad} is used in Equations (28) and (29) as the evolution of viscosity depends mainly on curing kinetic. The parameter η_0 is the initial viscosity at T_0 and K is the apparent kinetic factor which follows an Arrhenius law:

$$K(T) = K_0 \exp\left(\frac{E_K}{R_g}\left[\frac{1}{T_{\mathrm{ref}}} - \frac{1}{T}\right]\right) \tag{27}$$

The initial viscosity η_0 has been obtained by mixing the viscosities of each component of the PIW mixture (see Table 2). The first Arrhenius terms in Equations (12) or (13) are not considered because of the narrow range of initial temperatures ($23\,°C \leq T_0 \leq 34\,°C$). It is not possible to account for the fluidizing effect of gas bubbles (depicted by the function F_g) because the gas content in the experimental measurement range is very near the maximal gas content $\phi_{\max}$ (see Figure 6) but it could be introduced a posteriori using the parameters introduced by Bikard et al. [22], assuming that $F_g(\phi_{\max}) = 1$. The two parameters K_0 and E_K are determined by a least square method applied on data depicted by dashed lines in Fig. 5. The numerical values are reported in Table 2 for order 1 kinetics (Equation (28)) and order 2 kinetics reaction (Equation (29)), respectively. Figure 5 shows that both kinetics are consistent with the experimental viscosity measurements.

4.4 Summary

The PU foaming equations presented in section3 have been adapted in this section to the experimental conditions of the FOAMAT® device: namely, atmospheric pressure, nearly adiabatic condition during foaming. Therefore, we have introduced the variables ϕ_{free} and T_{ad} which correspond to the gas content at atmospheric pressure and adiabatic temperature respectively. These two new variables can be linked to the gas conversion rate α and curing conversion rate β respectively and the consistency with previous modelling approaches is then achieved.

The fitting procedure is rather standard as the problem is written as a minimization problem using the least square method. The fitting procedure of parameters $(T_m, K_{\text{ad}}, E_{\text{ad}}, c_f)$ in Equations (19-20), parameters $(\phi_{\max}, K_\phi, E_\phi, m_\phi, n_\phi)$ in Equation (24), and parameters (K_0, E_K) in Equations (28-30) or (29-30) can be computed independently but they are coupled with the temperature T. Therefore, an iterative procedure is added in order to get a better approximation of all parameters. These data will be applied in the next section to the numerical model of the FOAMAT® experiments. This will especially allow checking the validity of most of the numerous hypotheses used in section 4 for identifying kinetics and rheology parameters.

Initial density	$\rho_0\ (kg/m^3)$	1082	
Reference temperature	T_{ref} (°C)	21	Eq. (18,19,24)
Transfer coefficient	$c_f(\text{t}^{-1})$	3×10^{-4}	Eq. (16)
Maximal temperature	T_m(°C)	124.13	Eq. (19)
Curing coefficient	$K_{\text{ad}}(K.s^{-1})$	1.96	Eq. (19)
Activation energy of curing reaction on R	$E_{\text{ad}}/R\ (K)$	1.22×10^3	Eq. (19)
Maximal gas content	$\phi_{\max}$	0.971	Eq. (24)
Gas coefficient	$K_\phi\ (s^{-1})$	4.69×10^{-3}	Eq. (24)
Activation energy of gas conversion reaction on R	$E_\phi\ /R_g\ (K)$	1.07×10^4	Eq. (24)
Index n	n_ϕ	1.535	Eq. (24)
Index m	m_ϕ	0.094	Eq. (24)

Table 1: Values of kinetics parameters occurring in Equations (18), (19) and (24) obtained after fitting procedure

	$\eta_0\ (Pa.s)$	$K_0(s^{-1})$	$E_K\ /R_g$ (K)
Order 1 Eqs. (28,30)	0.748	5.74×10^{-3}	6.852×10^3
Order 2 Eqs. (29,30)	0.748	9.74×10^{-11}	4.5100×10^4

Table 2: Values of viscosity parameters occurring in Equations (28-30).

5. Numerical Computations of FOAMAT® experiments

In order to check the validity of the different hypotheses used for the identification of the parameters of the viscosity model and curing and foaming kinetics equations, a 3D simulation of the foaming process has been implemented in REM3D®, a software platform developed by Transvalor. In these computations, Equations (2-4) are coupled with the heat generation (19), the gas fractions (24) and viscosity evolution (28) and (30). The mass conservation equation has to be changed to account for the new variable ϕ_{free}. First, the gas content ϕ for an unknown pressure p is computed by assuming that the gas follows the ideal gas law. Writing $V_{foam} = V_g + V_{PU}$ with V_{PU} the volume of polyurethane matrix, the following relation is obtained between ϕ and $p(t), T(t), \phi_{free}(t)$:

$$\phi = \frac{p_a \ \phi_{\text{free}}}{p_a \ \phi_{\text{free}} + \ p\left(1 - \phi_{\text{free}}\right)} \tag{31}$$

and the mass balance (Equation (1)) is expressed as follows:

$$\nabla . \boldsymbol{u} = \frac{1}{1-\phi}\frac{d\phi}{dt} = \frac{1}{1-\phi}\left(\frac{\phi}{\phi_{\text{free}}}\right)^2 \frac{p}{p_a}\ \frac{d\phi_{\text{free}}}{dt} - \frac{\phi}{P}\frac{dp}{dt} - \frac{\phi}{T_{ad}}\ \frac{dT_{ad}}{dt} + \ \frac{\phi}{T}\ \frac{dT}{dt} \tag{28}$$

in which, the first term corresponds to the volume increase due to gas creation, the second term to pressure variation which can change bubble size and the last two terms to the temperature dependence of the bubble volume.

The parameters values are given in Tables 1 and 2. Please notice that the numerical computation has been done with adiabatic boundary condition along the cardboard wall and the bottom surface of the FOAMAT and the heat transfer coefficient h_T deduced from the identified c_f value (Table 1) along the free surface. The heat conductivity is function of the local gas content using the mixing rule as in ref. [12]. The chosen values are $\kappa_{PU} = 0.15\ W/mK$; $\kappa_{\phi} = 0.023\ \ W/mK$ and the heat capacity is constant in foam phase, $C_p = 1800\ J/kg\ K$

This set of equations is solved in a computational domain Ω (a cylinder in our case) with a finite element method. More precisely, all subdomains are embedded in a unique Eulerian mesh using the immersed volume method [51]. A level-set method [52] is used to get (i) implicit representation of the foam/air interface and (ii) proper definition of the viscosity η, the density ρ, the specific heat C_p and the thermal conductivity κ as space dependent functions. The level set is associated with the domain occupied by the foam (mixing liquid polyurethane and created gas). This level set function enables to properly describe the overall material functions in each sub-domain [53]. As explained in ref. [54], the level-set associated to the fluid/air interface is transported by the velocity solution of the above set of equations describing foam growth. In a first step, we justify some approximations of the analytical calculus. Then we compare the result of the direct numerical simulation with the experimental data.

5.1. Comparison between direct numerical simulation and analytical solution.

First, we check that the analytical model presented in the supplementary material, Section 3 to get the analytical formula of the viscosity (Equation (27)) agrees with the 3D computations. The main hypotheses state that the density and temperature are homogeneous in the volume at each time step and that the vertical velocity component is a linear function of the vertical component z (Eq. A-1 of the supplementary section).

The first assumption can be checked in Figures 7 in which the iso-values of temperature and density are reported for $t = 40\ s$ and an initial temperature $T_0 = 23\ °C$. The temperatures T as well as the density ρ are almost uniform in the whole cavity except in the vicinity of the outer boundary. The whole temperature T is computed accounting for the heat transfer between the foam/air interface above the top surface and the viscous dissipation whereas the temperature T_{ad} accounts only for the polymerization reaction. Figures 8 show the increase of temperature T (Figure 8a) and the correlated decrease of density ρ (Figure 8b) in the radial direction for two different vertical positions and at various times. Small temperature and density gradients near the cardboard wall are linked to the sticking contact at the wall and the fountain flow at the free surface. For example the adiabatic temperature is convected more slowly near the wall.

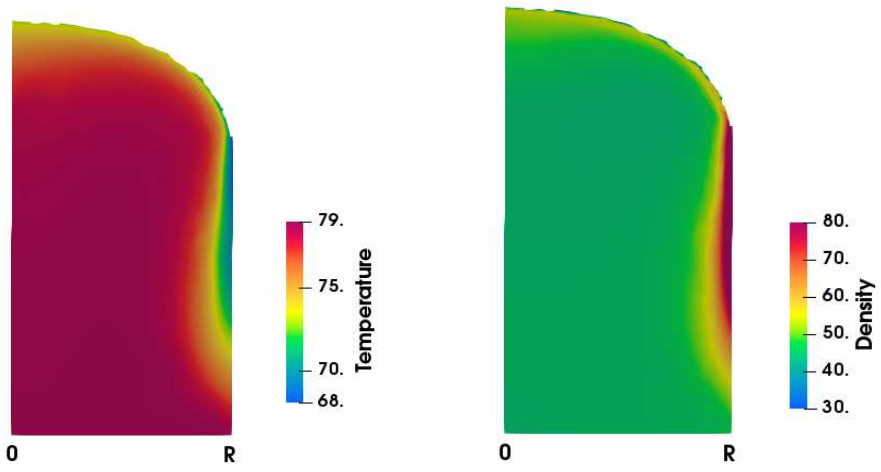

(a) *(b)*

FIGURE 7: Isovalues on vertical mid-plane for an initial temperature $T_0 = 23\ °C$ *and* $t = 40\ s$*: (a) temperature,* $T\ (°C)$*; (b) density,* $\rho\ (kg/m^3)$.

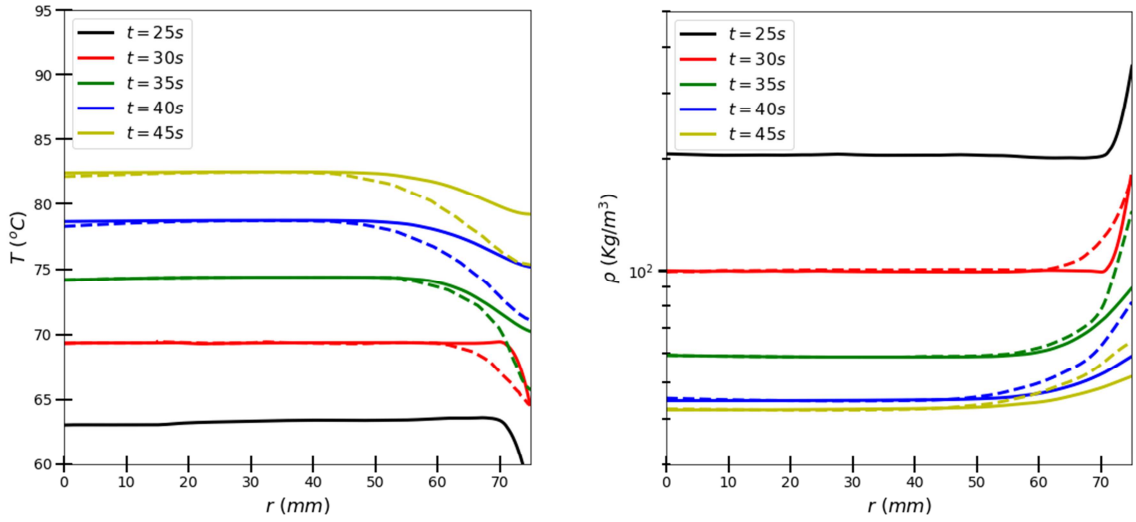

(a) *(b)*

FIGURE 8: Radial evolution at different times for vertical positions $z = 20\ mm$ *(plain lines) and* $z = 50\ mm$ *(dashed lines): (a) temperature* T (°C)*; (b) density* ρ (kg/m^3).

Figure 7 points also out the marked curvature of the free surface which has not been accounted for in the analytical model. In Figure 9, we compare the computed foam height at the symmetry axis with the one at the cardboard wall and the average foam height defined as $\bar{h} = V/S$ (the whole volume V filled by the foam divided by the surface S of the cylinder). It is interesting to notice that this last value is equivalent to the one obtained by introducing in REM3D® a perfect slip boundary condition at the cardboard wall. That means $\partial w/\partial r = 0$ instead of $w = 0$ on the outer boundary. This points out that the total amount of created gas does not depend on kinematics boundary conditions. Therefore, modeling the gas content evolution by measuring only the height in the middle of the cylinder is valid.

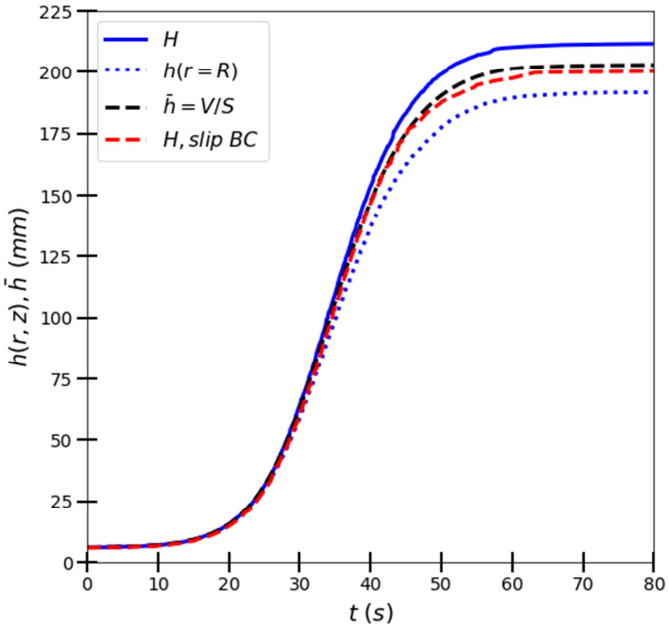

FIGURE 9: Time evolution of the foam height: $H = h(r = 0)$; $h(r = R)$; $\bar{h} = V/S$ and H = h(r=0) with slip boundary conditions.

The kinematic assumption is checked thanks to Figure 10. The computed vertical velocity component *w* is linear in *z* as in the analytical model developed in the supplementary material (Section 3), except in the vicinity of the upper surface where there is a fountain flow.

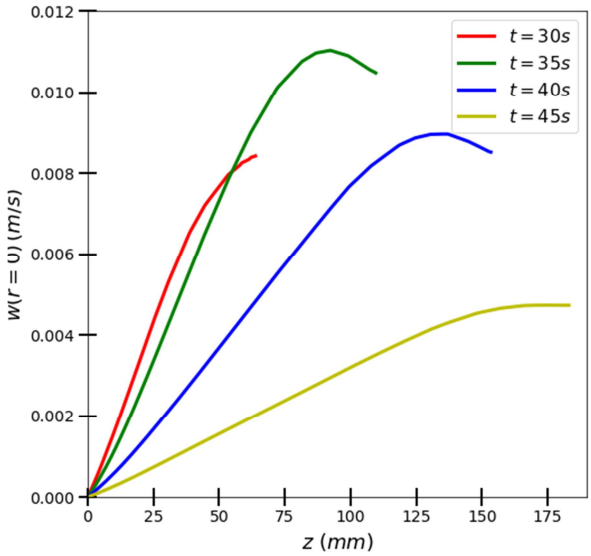

FIGURE 10: Evolution at different times of the vertical velocity w on the symmetry axis of the cavity.

5.2. Comparison between direct numerical simulation and experiments

Results of direct numerical computations are compared to solutions of the model (Section 4, Equations (19, 20, 24)) with parameters deduced from FOAMAT® measurements (Section 2). Thanks to the fitting procedure, these data are now known on a large time range. The results are reported in Figure 11 and show a good agreement between the modelling equations and direct numerical simulation.

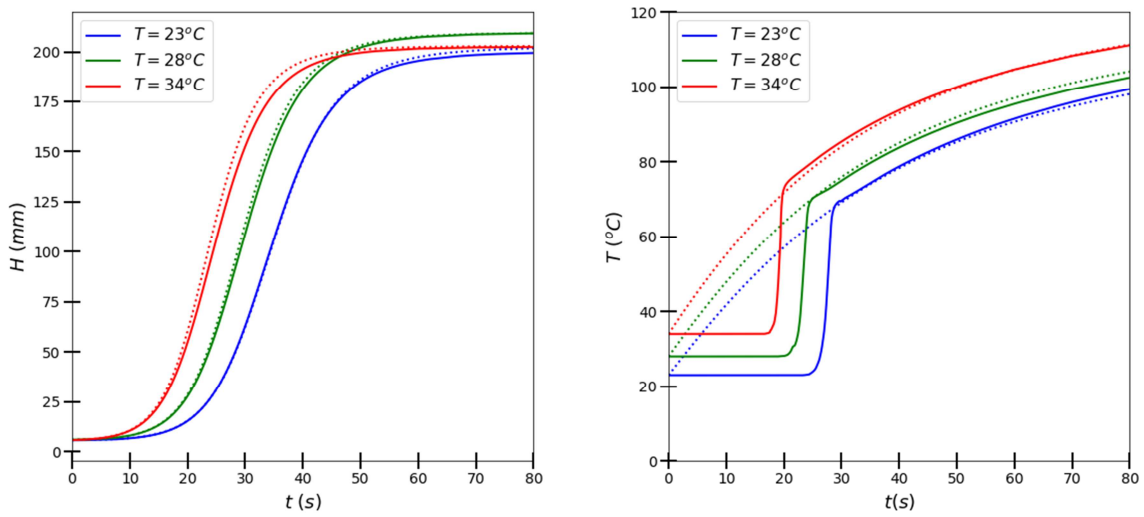

FIGURE 11: Comparison between numerical simulation (solid lines) and resolution of modeling equations (dotted lines) for the three initial temperatures: (a) evolution of the foam height; (b) evolution of the temperature at $z = 50\ mm$.

The influence of the initial viscosity η_0 is analyzed in the supplementary material (Section 5). It is shown that, multiplying the viscosity by a factor hundred (starting from the value obtained by the mixing rule of the viscosity of the components of the PIW mixture) does not influence the foam height development.

5. Conclusion

Modelling the foaming process of a polyurethane formulation requires identifying an important number of material parameters that are difficult to measure in classical rheological and thermodynamic set-ups, because the curing and foaming kinetics of most PU formulations are short in comparison with the characteristic times of the experimental measurements. The FOAMAT® set-up has been developed to overcome these limitations. It is a simple cylindrical geometry operated at ambient pressure with simple instrumentation. But the identification procedure to derive the parameter of the curing, foaming and viscosity equations was not properly developed. An analytical model developed in the supplementary material is proposed which allows identifying these parameters from foaming rise height, foaming velocity, temperature and stress measurements as a function of time. This analytical model is based on

several hypotheses: flat free surface, temperature and density uniformity at each time step, linear velocity profile in the vertical direction. The thermodynamics and rheological parameters are then used in a finite element simulation of the foaming process in the cylindrical geometry of the FOAMAT® device and in the processing conditions presented in Section 2. The numerical results are consistent with the experimental ones which justify the proposed identification procedure. In particular, the Castro-Macosko law (Equation (9)) which cannot be identified with FOAMAT® device can advantageously be replaced by Roller law. (Equation (28)).

It is to notice that the most important parameter is the maximum gas content ϕ_{max} at ambient pressure which governs the final foam density. The viscosity is important at the early stage in the industrial process when the mixture is injected in the mold. Its influence would be important at foaming completion for the transition between closed cells and opened cells. But, this latter effect is in fact measured by the ϕ_{max} parameter.

References

[1] M. Karimi, H. Droghetti and D. Marchisio, *Macromol. Symp.* **2016**, 360, 108.

[2] M. Karimi, H. Droghetti and D. Marchisio, *Computer Physics Communications* **2017**, 217, 138.

[3] D. Seo and J. Youn, *Polymer* **2005**, 46(117), 6482.

[4] N. Samkhaniani, A. Gharehbaghi and Z. Ahmadi, *J. Cellular Plastics* **2013**, 49(15), 405.

[5] G. Piloyan, I. Ryabchikov and O. Novikora, *Nature* **1966**, 212(15067), 1229.

[6] M. Kamal, *Polym. Eng. Sci.* **1974**, 14(13), 231.

[7] J. Castro and C. Macosko, *SPE ANTEC Tech. Papers* **1980**, 26, 434.

[8] M. Kamal and M. Ryan, *Adv. Polym. Technol.* **1984**, 4(13-4), 323.

[9] M. Roller, *Polymer Eng. Scien.* **1986**, 26(16), 432.

[10] F. Dimier, N. N. Sbirrazzuoli, B. Vergnes and M. Vincent, *Polym. Eng. Sci.* **2004**, 44(13), 518.

[11] R. Bouayad, J. Bikard and J.-F. Agassant, *Int. J. Mater. Form.* **2009**, 2, 243.

[12] I. E. Ireka, D. D. Niedziela, K. Schäfer, J. Tröltzsch, K. Steiner, F. Helbig, T. Chinyoka and L. Kroll, *Phys. Fluids* **2015**, 27, 113102-16.

[13] D. Seo, J. Youn and C. Tucker III, *Int. J. Numer. Meth. Fluids* **2003**, 42, 1105.

[14] R. Rao, L. Mondy, D. Noble, H. Moffat, D. Adolf and P. Notz, *Int. J. Numer. Meth. Fluids* **2011**, 68(111), 1362.

[15] P. Ferkl, M. Karimi, D. Marchisio and J. Kosek, *Chemical Engineering Science* **2016**, 148, 55.

[16] P. Ferkl, I. Kršková and J. Kosek, *Chemical Engineering Science* **2018**, 176, 50.

[17] D. Venerus and N. Nadia Yala, *AIChE Journal* **1997**, 43(111), 2948.

[18] D. Venerus, *Polym. Eng. Sci.* **2001**, 41(18), 1390.

[19] M. Roller, *Polymer Eng. Sci.* **1975**, 16, 406.

[20] M. Dusi, C. May and J. Seferis, *Chemorheology of Thermosetting Polymers* **1982**, 18, 301.

[21] D. Kim et C. Macosko, *Polym. Eng. Sci.* **2000**, 40(110), 2205.

[22] J. Bikard, J. Bruchon, T. Coupez and L. Silva, *Colloids and Surfaces A: Physicochem. Eng. Aspects* **2007**, 309(11-3), 49.

[23] J. Bikard, AM3714, *Techniques de l'Ingénieur* **2009**.

[24] R. Neff and C. Macosko, *Rheologica Acta* **1996**, 35, 656.

[25] E. Tuarez, P. Marchal, L. Choplin, *Int. J. of Adhes. Adhes.* **2014**, 50, 32.

[26] L. Choplin, P. Marchal, C. Baravian and D. Langevin, *Techniques de l'Ingénieur* **2010**, 1J 2145.

[27] M. Kuranska and A. Prociak, *Industrial Crops and Products* **2016**, 89, 182.

[28] A. Arafmanesh, S. Advani and E. Michaelides, *Polym. Eng. Sci.* **1990**, 30(120), 1330.

[29] L. Lefebvre and R. Keunings, In: M. Cross, J. F. T. Pittman, R. D. Wood (Eds) Mathematical modelling for Materials Processing, *Clarendon Press, Oxford* **1993**, 417.

[30] H. Abdessalam, B. Abbès, Y. Li, Y. Q. Guo, E. Kwassi and J.-L. Romain, *Mater. Res. Innovations* **2015,** 19(18),149.

[31] J. Feng and C. Bertelo, *J. Rheol.* **2004**, 48, 439.

[32] J. Bikard, J. Bruchon, T. Coupez and B. Vergnes, *J. Materials Sci.* **2005**, 40(122), 5875.

[33] J. Bruchon and T. Coupez, *Int. J. Numer. Meth. Fluids* **2008**, 57(8), 977.

[34] S. Geier and M. Piesche, *The Journal of Computational Multiphase Flows* **2014**, 6(14), 377.

[35] D. Niedziela, I. Ireka and K. Steiner, *MDPI* **2019**, 11(11), 100.

[36] R. Rao, L. Mondy, D. Noble, V. Brunini, K. Long, C. Roberts, N. Wyatt, M. Celina, K. Thompson and J. Tinsley, *Computers and Fluids* **2018**, 175, 20.

[37] J.-F Agassant, P. Avenas, P. Carreau, B. Vergnes, M. Vincent, *Polymer Processing 2E: Principles and Modeling*; Hanser, Inc., **2017**.

[38] H. Abdessalam, B. Abbès, Y. Li, Y.-Q. Guo, E. Kwassi and J.-L. Romain, *Int. J. Mater. Form.* **2016**, 9(11), 85.

[39] S. Baser and D. Khakhar, *Polym. Eng. Sci.* **1994**, 34(8), 632.

[40] S. Geier, C. Winkler and M. Piesche, *Chemical Engineering & Technology* **2009**, 32(19), 1438.

[41] G. Batchelor and J. Green, *J. Fluid. Mech.* **1972**, 56(13), 401.

[42] A. Kraynik and M. Hansen, *J. Rheology* **1987**, 31, 175.

[43] P. Sherman, *Rheol. Acta* **1962**, 2, 74.

[44] R. Prud'homme and S. Khan, In *Foams, Theory, measurements and applications*, New York, Marcel Dekker, Inc., **1996**, 217.

[45] D. Serrano, J. Peyrelasse, C. Boned, D. Harran and P. Monge, *J. Appl. Polym. Sci.* **1990**, 39, 679.

[46] J. Castro, C. Macosko, *AIChe J.* **1982**, 28(12), 250,.

[47] H. Winter, *Polym. Eng. Sci.* **1987**, 27, 1698,.

[48] K. Wang, Y. Huang and J. Lee, *Polym. Eng. Sci.* 1990, 30(111), 654.

[49] X. Sun, J. Toth, L. Lee, *Polym. Eng. Sci.* **1997**, 37(11), 143.

[50] K. Hollands and I. Kalnin, In *Epoxy Resins*, American Chemical Society **1970**, 92, 60.

[51] T. Coupez, H. Digonnet, E. Hachem, P. Laure, L. Silva, R. Valette, In *Arbitrary Lagrangian-Eulerian and Fluid–Structure Interaction*, Wiley, **2013**, 221.

[52] S. Osher and R. Fedkiw, Springer, **2003**.

[53] R. Nakhoul, P. Laure, L. Silva, M. Vincent, *Int. J. Material Forming* **2018**, 11(11), 53.

[54] L. Ville, L. Silva and T. Coupez, *Int. J. Numer. Meth. Fluids* **2011**, 66, 324.

[55] C. Kim and J. Youn, *Polym.-Plast. Technol. Eng.* **2000**, 39(11), 163.

Supplementary material

***Section 1**: Experimental measurement of the mean stress on the bottom surface of the FOAMAT® and temperature at 50 mm from the bottom surface on the same time scale.*

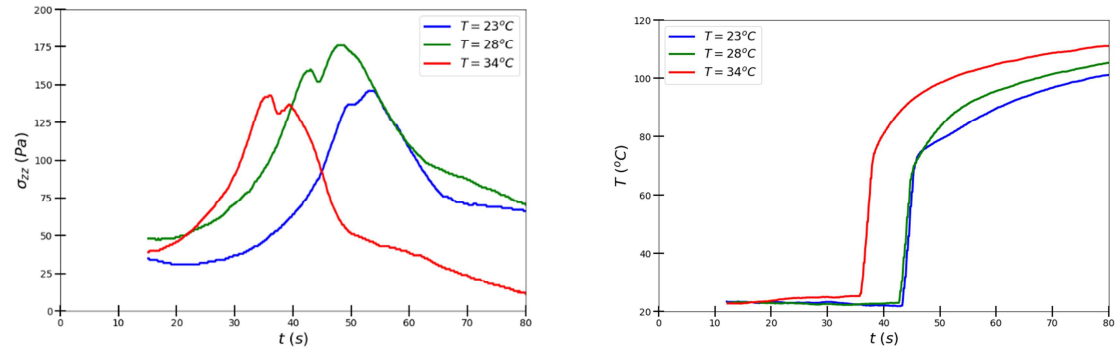

(a) *(b)*

Figure SM 1: Experimental stress (a) and temperature (b) measurements for three initial PIW temperatures.

Section 2: Identification of the gas content ϕ and of the conversion rate α as a function of time at the three different temperatures.

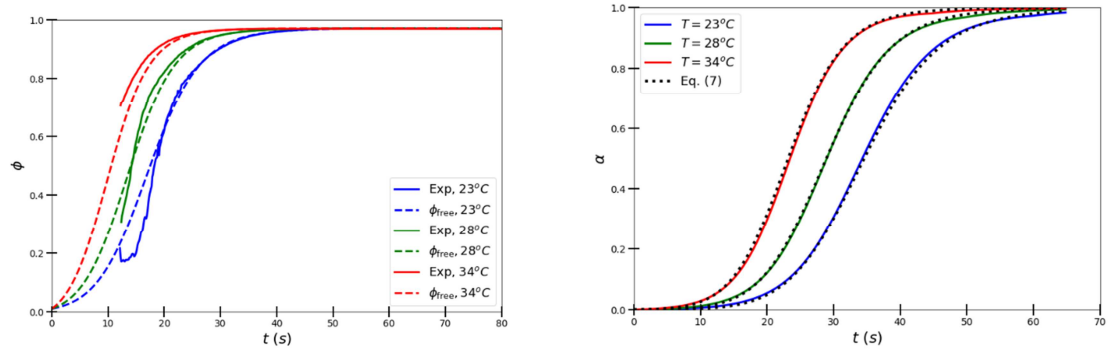

(a) *(b)*

Figure SM 2: (a) Experimental and fitted gas content with Equation 24; (b) Conversion rate α as a function of time for the three different temperatures: solid lines correspond to measured values (Equation (26)), dashed lines to fitted function (Equation (7)) with values given in Section 4.2.2 of the paper.

***Section 3**: Mechanical model of the foam expansion in the FOAMAT®*

*The velocity vector **u** writes in the cylindrical coordinate (r, θ, z) (see Figure 1)*

$$\boldsymbol{u} = \begin{bmatrix} u(r,z,t) \\ 0 \\ w(r,z) = z\,\varphi(r,t) \end{bmatrix} \tag{A-1}$$

The boundary conditions write:

$$\begin{aligned} u(R,z,t) = u(0,z,t) = 0 \\ \varphi(R,t) = \frac{\partial \varphi}{\partial r}(0,t) = 0 \end{aligned} \tag{A-2}$$

Although the foam/air interface $h(r,t)$ is not flat, the vertical velocity can be directly connected to velocity and height measured on the axis of symmetry:

$$w(0,h(0,t)) = \frac{d}{dt}[h(0,t)] = \frac{dH}{dt} \tag{A-3}$$

where $H(t) = h(0,t)$ is the interface position at the symmetry axis and dH/dt its velocity. These two quantities are recorded by the FOAMAT® and are plotted in Fig. 2a and Fig. 2c.

The mass balance equation (Equation (1)) becomes:

$$\frac{\partial \rho}{\partial t} + \rho\left(\frac{1}{r}\frac{\partial}{\partial r}(r\,u) + \varphi\right) = 0 \tag{A-4}$$

This leads to:

$$\frac{1}{r}\frac{\partial}{\partial r}(r\,u) + \varphi = -\frac{1}{\rho}\frac{d\rho}{dt} \tag{A-5}$$

If the density is uniform at each time step, the velocity component u is only a function of r at each time step: $u(r,t)$. The rate of strain tensor writes:

$$\dot{\varepsilon} = \begin{bmatrix} \frac{\partial u}{\partial r} & 0 & \frac{z}{2}\frac{\partial \varphi}{\partial r} \\ 0 & \frac{u}{r} & 0 \\ \frac{z}{2}\frac{\partial \varphi}{\partial r} & 0 & \varphi \end{bmatrix} \tag{A-7}$$

Introducing the stress tensor for a compressible Newtonian fluid (Equation (3)) in the momentum balance equation (Equation (2)), neglecting the inertia terms, leads to two differential equations:

$$\frac{\partial p}{\partial r} = \eta\,\frac{\partial \varphi}{\partial r} + 2\,\eta\frac{\partial}{\partial r}\left[\frac{1}{r}\frac{\partial}{\partial r}(r\,u)\right] \tag{A-8}$$

$$\frac{\partial p}{\partial z} = \eta\,z\frac{1}{r}\frac{\partial}{\partial r}\left[r\,\frac{\partial \varphi}{\partial r}\right] - \rho\,g \tag{A-9}$$

The derivative of Eq. (A-8) as a function of z is zero and so the derivative of Eq. (A-9) as a function of r leads to:

$$\frac{\partial^2 p}{\partial r\,\partial z} = \eta\,z\,\frac{\partial}{\partial r}\left[\frac{1}{r}\frac{\partial}{\partial r}\left(r\,\frac{\partial \varphi}{\partial r}\right)\right] = 0 \tag{A-10}$$

As a consequence:

$$\frac{1}{r}\frac{\partial}{\partial r}\left(r\ \frac{\partial \varphi}{\partial r}\right) = K(t) \tag{A-11}$$

and the boundary conditions (A-2) and (A-3) on φ and w gives:

$$K(t)\ = -\ \frac{4}{R^2}\frac{1}{H}\frac{dH}{dt} \quad \text{and} \quad \varphi(r,t) = \ -K(t)\frac{R^2 - r^2}{4} \tag{A-12}$$

Integrating Eq. (A-9) as a function of z and using Eq. (A-8) leads to:

$$p(r,z,t) = \frac{\eta}{2}z^2K(t) - \rho(t)g\ z + \ \eta\,\varphi(r,t) + 2\ \eta\ \frac{1}{r}\ \frac{\partial}{\partial r}(r\ u) + B(t) \tag{A-13}$$

Accounting for Eq. (A-5) this writes also:

$$p(r,z,t) = \ \frac{\eta}{2}\ z^2\ \ K(t)\ \ - \rho(t)\ g\ z - \eta\ \varphi(r,t) + p_0(t) \tag{A-14}$$

With $p_0(t) = B(t)\ -\ \frac{2}{\rho}\,\eta\frac{d\rho}{dt}$

The vertical stress $\sigma_{zz}(r,z,t)$ writes, according to the stress tensor for a compressible fluid (Equation (3)):

$$\begin{aligned}\sigma_{zz}(r,z,t) &= 2\eta\ \left(\varphi(r,t) + \ \frac{1}{3\,\rho}\frac{d\rho}{dt}\right) - p(r,z,t)\\ &= -\frac{\eta}{2}\ z^2\ \ K(t) + \rho(t)g\ z + 3\,\eta\ \varphi(r,t) - P_0(t)\end{aligned} \tag{A-15}$$

with $P_0(t) = -\,p_0(t)\ -2\ \eta\ \frac{1}{\rho}\frac{d\rho}{dt}$.

The stress is zero at the top of the free surface, $\sigma_{zz}(0,H,t) = 0$, which implies:

$$P_0(t) = -\frac{\eta}{2}\ K(t)\ H^2\ \ + \rho(t)g\ H + 3\ \eta\,\varphi(0,t) \tag{A-16}$$

Combining Equations (A-13) and (A-16) leads to the pressure distribution which writes along the symmetry axis:

$$p(0,z,t) = \frac{\eta}{2}\ K\ (\ z^2 - \ H^2) - \ \rho(t)g\ (z - H) + \frac{2\,\eta}{3}\ \frac{1}{\rho}\frac{d\rho}{dt} \tag{A-17}$$

Finally, the stress on the bottom surface is, according $\varphi(r,t)$ and $\varphi(0,t)$ given by Eq. (A-12):

$$\sigma_{zz}(r,0,t) = -\frac{\eta}{H}\ \frac{dH}{dt}\left[3\ \frac{r^2}{R^2} + 2\ \frac{H^2}{R^2}\right]\ -\ \rho(t)g\ H \tag{A-17}$$

The force transducer measures a mean value of the stress which writes:

$$\bar{\sigma}_{zz}(0,t) = \ \eta\frac{1}{H}\ \frac{dH}{dt}\left[2\ \frac{H^2}{R^2} + \ \frac{3}{2}\right] + \ \rho(t)g\ H \tag{A-18}$$

The viscosity is deduced from the measurements as a function of time of the average stress $\bar{\sigma}_{zz}(0,t)$, of the foam height $H(t)$ and of the foam rise velocity (dH/dt):

$$\eta(t) = \frac{\bar{\sigma}_{zz}(0,t) - \rho(t) g\, H(t)}{\frac{1}{H(t)} \frac{dH(t)}{dt} \left[2\, \frac{H^2(t)}{R^2} + \frac{3}{2} \right]} \tag{A-19}$$

Assuming that the mass of the PIW mixture, m, remains constant, Eq. (A-19) writes:

$$\eta(t) = \frac{\bar{\sigma}_{zz}(0,t) - \frac{m\, g}{\pi\, R^2}}{\frac{1}{H(t)} \frac{dH(t)}{dt} \left[2\, \frac{H^2(t)}{R^2} + \frac{3}{2} \right]} \tag{A-20}$$

Section 4: Comparison between analytical and computed pressure along the axis of symmetry of the FOAMAT®

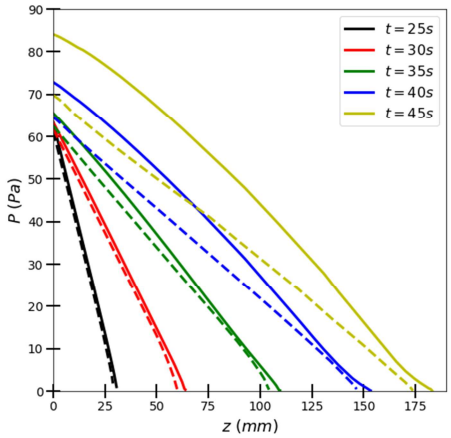

Figure SM3: Evolution of the pressure along the symmetry axis of the Foamat at successive time steps. The continuous line corresponds to the sticking contact; the dashed line to the slipping contact.

The pressure profile is parabolic as calculated by Eq. (A-17), but the second term of the equation is dominant which means that it seems to be linear.

Section 5: Test of the initial viscosity η_0

Direct numerical computations are made for different values of $\eta_0 = 7.48; 0.748; 0.0748$ $(Pa.s)$. The lowest value corresponds to the mixture law between the different components of the PIW mixture. Figure SM4a points out that, even if the foam height in the middle of the cavity is higher for a larger value of η_0, the mean value $\bar{h}$ remains very similar. In addition, Figure SM4b shows that this initial change on viscosity modifies largely the viscosity during the foaming. Therefore, the viscosity has a minor influence on the foaming process and the final density of the foam.

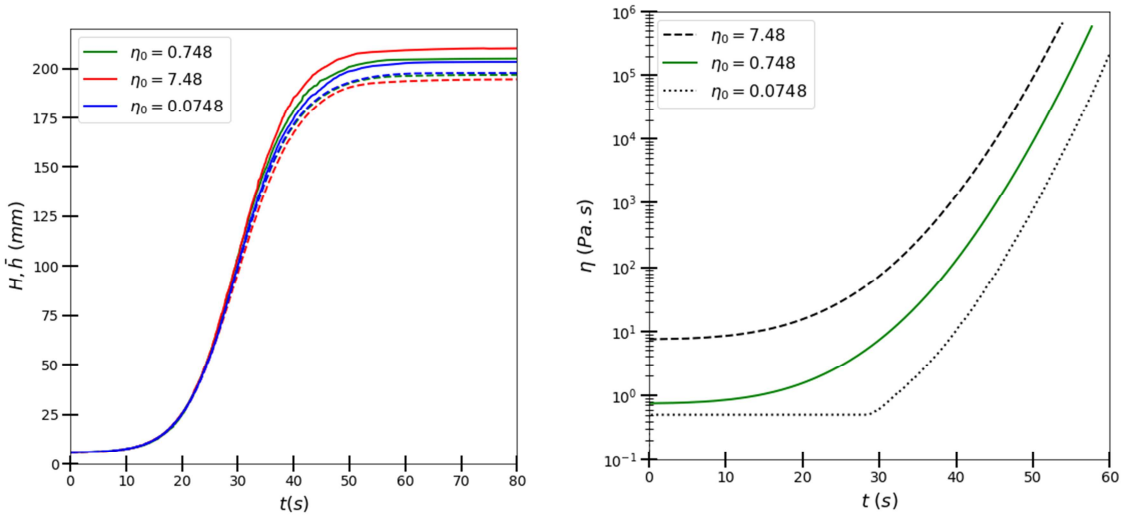

(a) (b)

FIGURE SM4: Influence of initial viscosity η_0 for an initial temperature $T_0 = 28\,°C$: (a) Evolution of foam height H (plain lines) and mean foam height $\bar{h}$ (dashed lines); (b) evolution of computed viscosity at vertical location $z = 5$